Chapter 2

2-D Theory

In this chapter I introduce the theory behind the LSJIMP method. The chapter is divided into three sections. In section 2.1 I motivate the LSJIMP inverse problem in general. In Section 2.2, I go on to outline my particular implementation of LSJIMP. In section 2.2.2, I show how, in a laterally-homogeneous earth, to create prestack time-domain images of pegleg multiples that are directly comparable, both in terms of kinematics and amplitudes, to the image of the primaries. In a heterogeneous earth, peglegs "split" into multiple arrivals. To account for this phenonmenon, in section 2.2.6 I introduce the HEMNO (Heterogeneous Earth NMO Operator) equation, which can independently image each leg of split peglegs in a moderately heterogeneous earth.

2.1 The LSJIMP Inverse problem

Figure 1.3 motivates LSJIMP. The Figure assumes that the recorded data is the superposition of primary events and pegleg multiples from the seabed. In effect, the images constructed from the primaries and from each mode of multiple constitute independent measurements of the earth's reflectivity at depth. Unfortunately, these independent measurements are embedded in a single data record. We would like to improve signal-to-noise ratio or fill illumination gaps by averaging the images. However, simple averaging of the raw images encounters two problems.

First, unless the multiple images have undergone an appropriate amplitude correction, the signal events are incommensurable. Secondly, corresponding crosstalk events on the primary and multiple images are kinematically quite consistent, especially at near offsets, meaning that averaging the images will do little to increase the signal-to-noise ratio or signal fidelity.

The previous paragraph underscores the main obstacle facing algorithms which attempt to jointly image multiples and primaries: while multiples provide additional information about the earth's reflectivity, we cannot exploit it unless we separate the individual modes. Cleanly separating a variety of different multiple modes from prestack data is both expensive and difficult. Moreover, by casting mode separation as a preprocessing step, as is the norm, we risk biasing the amplitudes in the separated modes, which could inhibit the integration.

LSJIMP solves the separation and integration problems simultaneously, as a global least-squares inversion problem. The model space, as illustrated in Figure 1.3, contains a collection of images, with the energy from each mode partitioned into one, and only one image. Moreover, each image has a special form: because the forward modeling operator contains appropriate amplitude correction operators the signal events in multiple and primary images are directly comparable, in terms of both kinematics and amplitudes. In order to solve the integration problem, we can apply a model regularization operator which penalizes inconsistency between images, and thus "spreads" signal from one model panel to another, using the multiples to fill gaps in the primary illumination and to increase signal fidelity.

LSJIMP models the recorded data as the superposition of primary reflections and p orders of pegleg multiples from n_{surf} multiple-generating surfaces. An i^{th} order pegleg splits into $i+1$ legs. If we denote the primaries as $\mathbf{d}_0$ and the k^{th} leg of the i^{th} order pegleg from the m^{th} multiple generator as $\mathbf{d}_{i,k,m}$, the modeled data takes the following form:

$$\mathbf{d}_{\text{mod}} = \mathbf{d}_0 + \sum_{i=1}^{p} \sum_{k=0}^{i} \sum_{m=1}^{n_{\text{surf}}} \mathbf{d}_{i,k,m}. \tag{2.1}$$

Figure 1.3 illustrates a simple case, where we model only first-order peglegs from a the seabed ($p = n_{\text{surf}} = 1$).

Other authors have solved a similar least-squares problem. Nemeth et al. (1999) jointly imaged and separated compressional waves and various (non-multiple) embedded coherent noise modes. Guitton et al. (2001) used nonstationary prediction-error filters to model primaries and surface-related multiples, but cast the problem purely in terms of wavefield separation, rather than joint imaging of multiples and primaries.

If we have designed an imaging operator that produces primary and multiple images with consistent signal (kinematics and angle-dependent amplitudes), then we assume that we can model the important events in the data. Let us denote the modeling operator (adjoint to imaging) for primaries $\mathbf{L}_0$ and the image of the primaries $\mathbf{m}_0$. Similarly, for the k^{th} leg of the i^{th} order pegleg from the m^{th} multiple generator, we denote the modeling operator and image $\mathbf{L}_{i,k,m}$ and $\mathbf{m}_{i,k,m}$, respectively. Following Figure 1.3, we can rewrite equation (2.1):

$$\mathbf{d}_{\text{mod}} = \mathbf{L}_0\mathbf{m}_0 + \sum_{i=1}^{p}\sum_{k=0}^{i}\sum_{m=1}^{n_{\text{surf}}}\mathbf{L}_{i,k,m}\mathbf{m}_{i,k,m} \tag{2.2}$$

$$= \mathbf{L}\mathbf{m} \tag{2.3}$$

2.1.1 LSJIMP: Least-squares minimization

The LSJIMP method seeks to optimize the primary and multiple images, $\mathbf{m}$, by minimizing the ℓ_2 norm of the data residual, defined as the difference between the recorded data, $\mathbf{d}$, and the modeled data, $\mathbf{d}_{\text{mod}}$ [equation (2.3)]:

$$\min_{\mathbf{m}} \|\mathbf{d} - \mathbf{L}\mathbf{m}\|^2. \tag{2.4}$$

Minimization (2.4) is under-determined, for many choices of prestack imaging operator, which implies an infinite number of least-squares-optimal solutions. Practically speaking, this problem manifests itself as crosstalk leakage. If (for instance) $\mathbf{m}_0$ contains residual first-order pegleg multiple energy, equation (2.1) will map this energy back into data space, at the position of a first-order multiple. Minimization (2.4) alone cannot distinguish between crosstalk and signal.

Of this infinity of possible $\mathbf{m}$'s, we seek the one which not only fits the recorded data, but

which also has minimum crosstalk leakage and maximum consistency between signal events on different images. In section 2.1.3 I introduce model regularization operators to accomplish both goals.

After the minimization of equation (2.4), theory dictates that the data residual should be independent and identically distributed (iid), or more intuitively, uncorrelated and evenly scaled. Correlated events in the residual imply that the forward model, $\mathbf{L}$, poorly models or fails to model events in the data. Examples of poor scaling might be the loss of reflection strength for deep reflectors, or empty traces. In general we compensate for a correlated or poorly scaled data residual by adding a residual weighting operator, $\mathbf{W_d}$:

$$\min_{\mathbf{m}} \ \| \mathbf{W_d} \left[\mathbf{d} - \mathbf{L}\mathbf{m} \right] \|^2, \tag{2.5}$$

where strictly speaking,

$$\left(\mathbf{W_d}^T \mathbf{W_d} \right)^{-1} = \mathrm{cov}[\mathbf{d}], \tag{2.6}$$

although in my implementation of LSJIMP, outlined in section 2.2, a far simpler choice for $\mathbf{W_d}$ is used.

2.1.2 LSJIMP: Choice of Imaging Operator

The exact form of the modeling operators, $\mathbf{L}_{i,k,m}$, shown in equation (2.3) has not yet been discussed. Any candidate prestack imaging operator for multiples must accomplish two tasks: focus the multiples in time/depth and offset/angle at the position of the primary and correct their amplitude to make the multiples directly comparable to the corresponding primary.

The literature contains many multiple modeling techniques which use wavefield extrapolation to "add a multiple bounce" to recorded data, and thus transform primaries into a model of the multiples, which is then generally adaptively subtracted from the data. These modeling techniques can roughly be divided into earth-model-based (Morley, 1982; Berryhill and Kim, 1986; Wiggins, 1988; Lu et al., 1999) and autoconvolutional (Riley and Claerbout, 1976; Tsai, 1985; Verschuur et al., 1992) approaches. It is possible to reverse the multiple modeling

process–in other words, to "remove a multiple bounce" from the data and transform multiples into pseudo-primary events, which can then be imaged as primaries (Berkhout and Verschuur, 2003; Shan, 2003).

Existing migration techniques for multiples perform the reverse modeling process either explicitly (i.e., using an earth model) or implicitly. Reiter et al. (1991) imaged pegleg multiples with Kirchhoff prestack depth migration. He and Schuster (2003) present a least-squares joint imaging scheme for multiples that uses poststack Kirchhoff depth migration. Yu and Schuster (2001) and Guitton (2002) migrate peglegs with shot-profile depth migration, while Berkhout and Verschuur (1994) used a similar crosscorrelation technique. Shan (2003) uses source-geophone migration after crosscorrelation at the surface. None of these techniques explicitly addresses the issue of amplitudes, beyond a polarity flip.

In this thesis, I use an earth-model-based multiple modeling strategy to simulate the kinematics and angle-dependent amplitude behavior of pegleg multiples. In section 2.2.1 I derive an extension to the normal moveout (NMO) equation for pegleg multiples. In section 2.2.6 I introduce HEMNO (Heterogeneous Earth Multiple NMO Operator), an extension of the NMO equation for multiples, which independently images split peglegs in a moderately heterogeneous earth. In Sections 2.2.2-2.2.5 I derive a series of amplitude correction operators to normalize the angle-dependent reflectivity of imaged multiples to be commensurable with their imaged primaries.

I postpone giving the full motivation for my particular choice of multiple imaging operator, as well as many implementation details until section 2.2. However, we can at this early stage state some important facts which have bearing on how the problem is regularized and how it is implemented computationally. The prestack multiple image, $\mathbf{m}_{i,k,m}$, shown in Figure 1.3, is parameterized by zero-offset traveltime, τ, offset, x, and midpoint, y. However, one important feature of the my combined imaging operator is the fact that it operates on a CMP-by-CMP basis. This underscores the fact that HEMNO applies a vertical stretch, and does not move information across midpoint. The regularization schemes I present also do not operate across midpoint. This implementation allows a coarse-grained parallelization scheme, enabling straightforward parallel computation on a Linux cluster.

2.1.3 Regularization of the LSJIMP Problem

In Sections 2.1.4-2.1.6, I exploit three discriminants between crosstalk and signal to devise model regularization operators. The raw LSJIMP minimization [equation (2.5)] suffers from non-uniqueness. The model regularization operators choose the particular set of primary and multiple images which are optimally free of crosstalk, from an infinite number of possible combinations. Moreover, these operators exploit signal multiplicity–within and between images–to increase signal fidelity and fill illumination gaps/missing traces. Some existing regularized least-squares prestack migration schemes exploit signal multiplicity across reflection angle (Kuehl and Sacchi, 2001; Prucha and Biondi, 2002; Wang et al., 2003). LSJIMP's additional use of multiples to regularize the least-squares imaging problem is novel.

As mentioned in the previous section, my particular implementation of LSJIMP processes each CMP location independently. Therefore, without loss of generality, the regularization terms described in the following sections assume that the prestack multiple images, $\mathbf{m}_{i,k,m}$, are functions of zero-offset traveltime (τ) and offset (x), but not of midpoint. The same logic applies to an image parameterized by depth and reflection angle.

2.1.4 Regularization 1: Differencing between images

Corresponding signal events on all $\mathbf{m}_{i,k,m}(\tau,x)$ are focused at a single τ for all x, and by design, have directly comparable amplitudes. Conversely, corresponding crosstalk events on two model panels (e.g. residual first-order multiples on $\mathbf{m}_0$ and residual second-order multiples on $\mathbf{m}_{1,k,m}$) generally have different residual moveout. While the exact magnitude of the moveout differences depend on the choice of imaging operator, Figure 2.1 illustrates that they generally are small at near offsets, but more pronounced in the presence of subsurface complexity, and at far offsets/reflection angles.

We therefore conclude that at fixed (τ,x), the difference between two $\mathbf{m}_{i,k,m}$ will be relatively small where there is signal, but large where there is crosstalk noise. We now write this

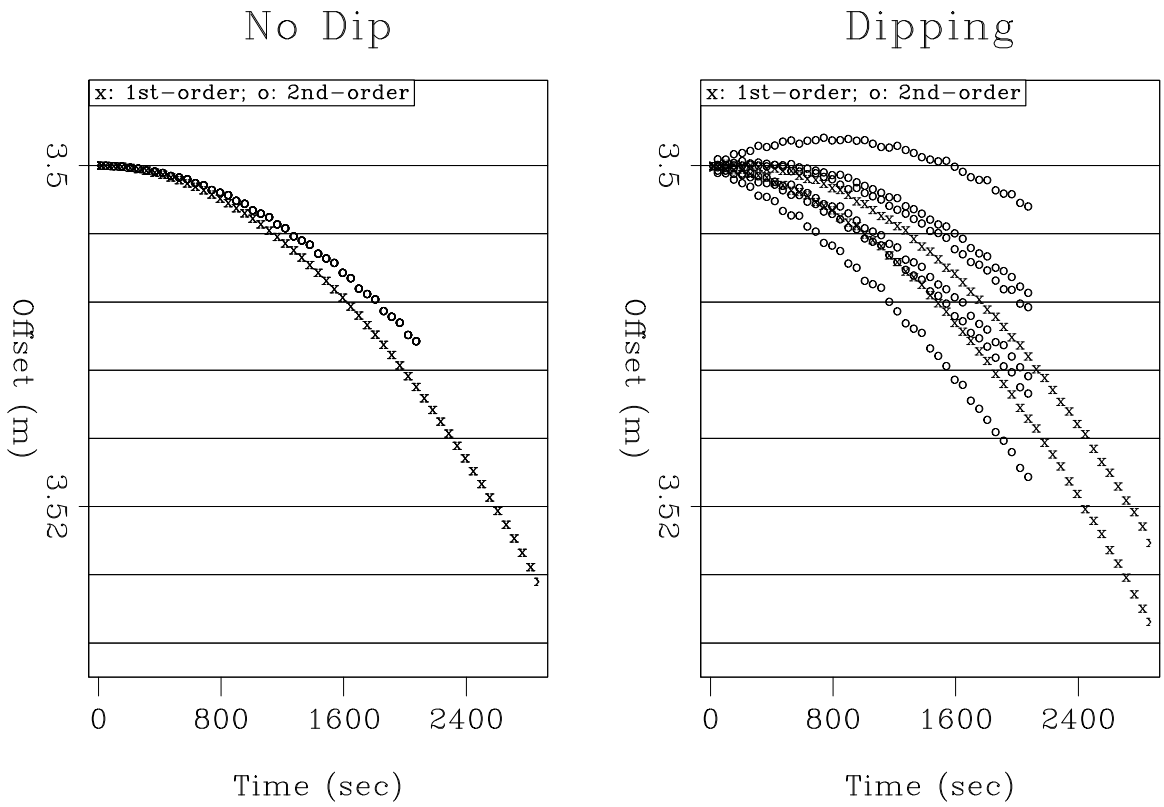

Figure 2.1: Comparison of crosstalk events on primary and first-order multiple images, for my particular choice of multiple imaging operator. "X" indicates position of split first-order pegleg on primary image, $\mathbf{m}_0$. "o" indicates position of the three second-order pegleg events on both $\mathbf{m}_{1,0,1}$ and $\mathbf{m}_{1,1,1}$. Left panel is with no subsurface dip, right has seabed and target reflector dip of 4°. With no dip, corresponding crosstalk events have little differential moveout. A small amount of dip quickly increases differential moveout. theory2d-crossdiff2.gulf [ER]

difference as a model residual:

$$\mathbf{r}_m^{[1]}[j](\tau,x) = \mathbf{m}_j(\tau,x) - \mathbf{m}_{j+1}(\tau,x), \quad \text{where} \quad j = [0, p(p+3)/2]. \tag{2.7}$$

p is the maximum order of multiple included in equation (2.2). Here I have modified the notation a bit and written $\mathbf{m}_j$ rather than $\mathbf{m}_{i,k,m}$ because the difference (2.7) is blind to the order or leg of the pegleg corresponding to $\mathbf{m}_j$; it is simply a straight difference across all the model panels.

As mentioned early in this thesis, a central motivation for LSJIMP is the desire to combine information from the multiple and primary images by averaging. In addition to discriminating against crosstalk, equation (2.7) provides a systematic framework for this averaging. If a signal event on one image is obscured by noise, the noise may not be present on an adjacent image, and equation (2.7) will attenuate it. This regularization enforces a degree of smoothness and consistency between images.

2.1.5 Regularization 2: Differencing across offset

After imaging with the correct velocity, signal events on all $\mathbf{m}_{i,k,m}$ are flat, while crosstalk events have at least some residual curvature, especially at far offsets and in regions with a strong velocity gradient. Provided that the AVO response of the signal changes slowly with offset, the difference (in offset) between adjacent samples of any $\mathbf{m}_{i,k,m}$ will be relatively small where there is signal, but large where there is crosstalk noise. We again cast this difference as a model residual:

$$\mathbf{r}_m^{[2]}[i,k,m](\tau,x) = \mathbf{m}_{i,k,m}(\tau,x) - \mathbf{m}_{i,k,m}(\tau,x+\Delta x). \tag{2.8}$$

2.1.6 Regularization 3: Crosstalk penalty weights

The third and final discriminant between crosstalk and signal exploits the inherent predictability of the crosstalk to suppress it. If we have an estimate of the signal, we can directly model

the expected crosstalk events on each $\mathbf{m}_{i,k,m}$, and construct a model-space weighting function to penalize crosstalk. Unfortunately, unless we employ a nonlinear iteration (see section 2.1.8), we do not, a priori, have this signal estimate. However, between the seabed reflection and the onset of its first multiple, the recorded data contains only primaries (inter-bed multiples and locally-converted shear waves are generally weak), and it is these strong, shallow events that often spawn the most troublesome crosstalk events. Therefore, we can directly model any pegleg multiple arising from a multiple generator with traveltime less than that of the first seabed multiple.

If we define $\mathbf{M}_0$ as an operator that applies a flat mute below twice the zero-offset traveltime of the seabed, and $\mathbf{M}_i$ as a similar operator that mutes above the zero-offset traveltime of the i^{th} multiple generator, then

$$\mathbf{z}_{i,k,m} = \mathbf{L}_{i,k,m}\mathbf{M}_{i,m}\mathbf{M}_0\mathbf{L}_0^T\mathbf{d} \tag{2.9}$$

is a model of the k^{th} leg of the i^{th} order multiple from the m^{th} multiple generator. Each $\mathbf{m}_{i,k,m}$ in equation (2.2) should ideally contain only the k^{th} leg of the i^{th}-order multiple from the m^{th} multiple generator – all other energy is crosstalk. To simulate crosstalk noise in $\mathbf{m}_{i,k,m}$, we apply $\mathbf{L}_{i,k,m}$ to all multiple model panels $\mathbf{z}$ (except $\mathbf{z}_{i,k,m}$) and sum:

$$\mathbf{c}_{l,n,q} = \sum_{j=l_0}^{p}\sum_{k=0}^{j}\sum_{m=1}^{n_{\text{surf}}}\mathbf{L}_{l,n,q}^T\mathbf{z}_{j,k,m}, \text{ where } k \neq n,\ m \neq q \text{ and } l_0 = \begin{cases} 1 & \text{if } l = 0 \\ l & \text{otherwise} \end{cases} \tag{2.10}$$

$\mathbf{c}_{i,k,m}$ is a kinematic model of crosstalk for $\mathbf{m}_{i,k,m}$. It could be used as a traditional multiple model (see section 3.1) and subtracted from the data, but I instead convert each $\mathbf{c}_{i,k,m}$ into a weighting function by taking the absolute value. We can write the model residual corresponding to the third model regularization operator:

$$\mathbf{r}_m^{[3]}[i,k,m](\tau,x) = \left|\mathbf{c}_{i,k,m}(\tau,x)\right|\ \mathbf{m}_{i,k,m}(\tau,x). \tag{2.11}$$

Although the crosstalk weights will likely overlap (and damage) signal to some extent, the signal's flatness and self-consistency between images ensures that regularization operators (2.7) and (2.8) will "spread" redundant information about the primaries from other $\mathbf{m}_{i,k,m}$ and

other offsets to compensate for any losses. Figure 2.2 illustrates the application of the crosstalk weights for the primary image and a multiple image. On panel (a), the primary image, the crosstalk is the obviously curving events. On panel (c), the seabed pegleg image, the crosstalk events are multiples from other multiple generators (e.g., R1M and R2M). Notice that in both cases the unwanted multiples are picked cleanly out of the data, leaving the underlying signal intact.

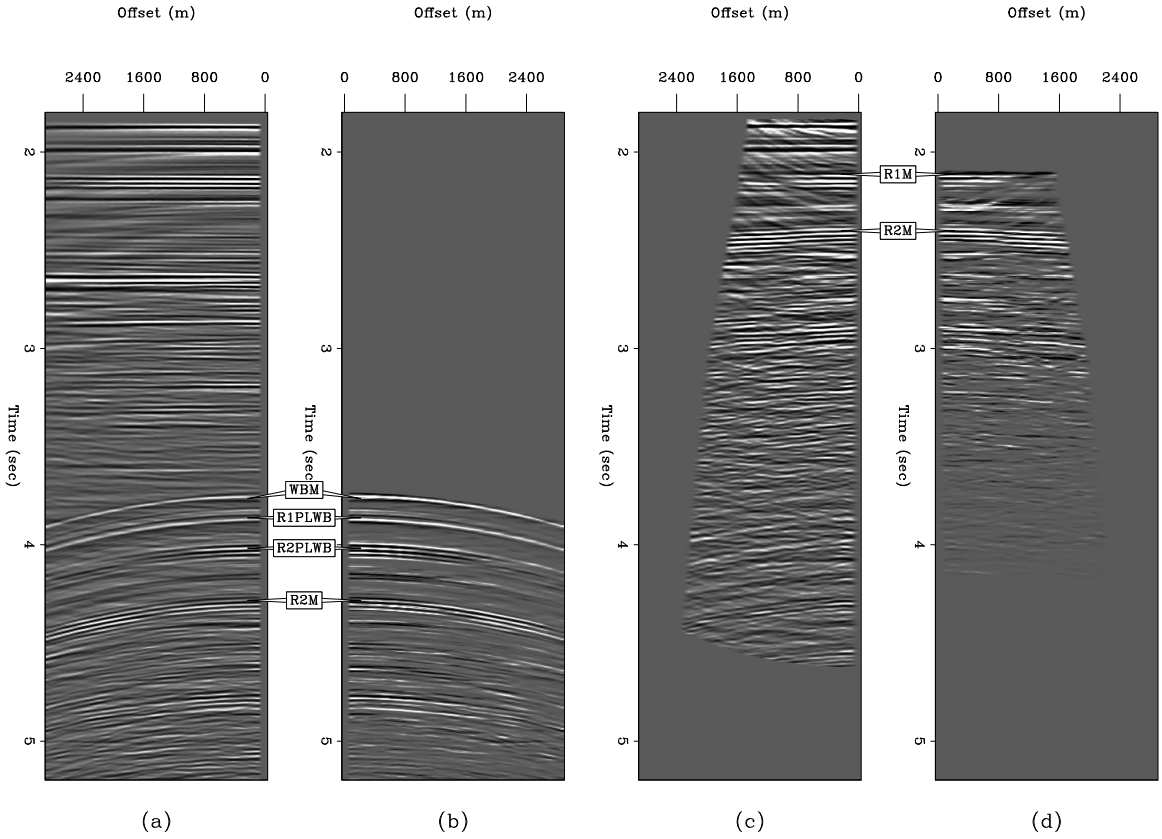

Figure 2.2: Application of crosstalk weights to real CMP after prestack imaging. Panel (a): primary image, $\mathbf{L}_0^T\mathbf{d}$. Panel (b): weighted primary image, $|\mathbf{c}_0|\mathbf{L}_0^T\mathbf{d}$. Panel (c): seabed pegleg image, $\mathbf{L}_{1,0,1}^T\mathbf{d}$. Panel (d): weighted seabed pegleg image, $|\mathbf{c}_{1,0,1}|\mathbf{L}_{1,0,1}^T\mathbf{d}$. $n_{\text{surf}} = 4$ in this case. Prominent crosstalk events are labeled on the various panels. theory2d-crosstalk.gulf [CR,M]

2.1.7 Combined LSJIMP Data and Model Residuals

To effect the final step of LSJIMP, the estimation of the optimal set of $\mathbf{m}_{i,k,m}$, we minimize a quadratic objective function which consists of the sum of the weighted ℓ_2 norms of the data residual [equation (2.5)] and of the three model residuals [equations (2.7), (2.8), and (2.11)]:

$$\min_{\mathbf{m}} Q(\mathbf{m}) = \|\mathbf{W_d}\,[\mathbf{Lm}-\mathbf{d}]\|^2 + \epsilon_1^2\|\mathbf{r}_m^{[1]}\|^2 + \epsilon_2^2\|\mathbf{r}_m^{[2]}\|^2 + \epsilon_3^2\|\mathbf{r}_m^{[3]}\|^2. \qquad (2.12)$$

ϵ_1, ϵ_2, and ϵ_3 are scalars which balance the relative weight of the three model residuals with the data residual. For the large scale problems endemic to seismic imaging, the conjugate gradient method is a logical choice to minimize $Q(\mathbf{m})$.

2.1.8 LSJIMP Nonlinear Iterations

Proponents of so-called "full-waveform inversion" (Tarantola, 1984) seek to solve an ambitious nonlinear inverse problem. In the context of reflection seismology, full-waveform techniques seek to invert a relation of the following qualitative form:

$$\text{recorded data} \quad = \quad \mathcal{L}\,(\text{density, velocity})$$

Most generally, the operator $\mathcal{L}$ is elastic two-way wave equation modeling, although making the acoustic assumption simplifies matters. In both cases, the modeling operator is nonlinearly dependent on the earth model to be estimated. For many reasons (including, but not limited to: computational expense, model non-uniqueness/nullspace, and sensitivity to starting model), full-waveform techniques are rarely applied successfully in today's conventional seismic processing environment. The LSJIMP method can be abstracted in a similar qualitative fashion, using the notation of the previous sections:

$$\begin{aligned} \mathbf{L} &\Leftarrow \text{velocity, reflection coefficient, crosstalk model} \\ \mathbf{d} &= \mathbf{Lm} \end{aligned}$$

Quantities like imaging velocity, the measured reflection coefficient of the multiple generators, and the crosstalk model are assumed to be fixed. Some LSJIMP implementations might depend only implicitly on velocity or reflection coefficient. For the sake of argument, however, let us assume that the LSJIMP operator, $\mathbf{L}$, is a non-linear function of these parameters, which the basic LSJIMP inversion makes no attempt to optimize. A multiple-free estimate of the primaries obviously enhances our ability to estimate imaging velocity, regardless of the method, and also permits us to model crosstalk noise from primaries that are below the onset of the seabed pure multiple. Thus the simplest nonlinear iteration of the LSJIMP method would proceed as follows, where the superscript k denotes that an operator or model vector is attached to the k^{th} nonlinear iteration:

iterate {

$\mathbf{L}^{[k]} \quad \Leftarrow \quad$ velocity, reflection coefficients, crosstalk model

$\mathbf{d} \quad = \quad \mathbf{L}^{[k]}\mathbf{m}^{[k]}$

$\mathbf{m}^{[k]} \quad \Rightarrow \quad$ updated velocity, crosstalk model

}

Nonlinear updating of the reflection coefficients of the multiple generators is in general a more difficult, and potentially more valuable, problem. If a multiple generator's pure multiple is obscured by other events, the reflection coefficient estimation scheme outlined in section 2.2.5 may produce inaccurate estimates, which the spatial regularization may not account for. For example, in the 2-D field data example shown in Chapter 3, the pure multiple for one multiple generator happens to be overlapped over almost the entire line by a prominent pegleg from another multiple generator.

I propose a nonlinear reflection coefficient updating scheme which obtains perturbations by fitting unmodeled events in the LSJIMP data residual, $\mathbf{r}_d$. If the initial reflection coefficient is perfect, then after convergence, $\mathbf{r}_d$ will contain only uncorrelated noise. If it is imperfect, then we also expect to see correlated events left over in the residual. Because LSJIMP separates each multiple mode indpendently in the model space ($\mathbf{m}_{i,k,m}$), we can simply apply the forward model for that mode ($\mathbf{L}_{i,k,m}$) to obtain an estimate of the particular multiple in data space, $\mathbf{d}_{i,k,m}$.

The main idea of my updating scheme is to compute a scalar update to the reflection coefficient of the m^{th} multiple generator, $\Delta\alpha_m$, such that

$$\|\mathbf{r}_d - \Delta\alpha_m\, \mathbf{d}_{i,k,m}\|^2 \tag{2.13}$$

is minimized. Since $\mathbf{r}_d$ may contain correlated events from primaries and other multiple modes, I suggest using $\mathbf{d}_{i,k,m}$ to compute a residual weight which is large where $\mathbf{d}_{i,k,m}$ is energetic, small where it is not. Using the absolute value of $\mathbf{d}_{i,k,m}$ is one possibility:

$$\left\| \left|\mathbf{d}_{i,k,m}\right| \left(\mathbf{r}_d - \Delta\alpha_m\, \mathbf{d}_{i,k,m}\right) \right\|^2. \tag{2.14}$$

In the implementation of minimization (2.14) used in this thesis, $\Delta\alpha_m$ is computed independently at each midpoint location, y. The updated reflection coefficient, $\alpha_m^{[k]}(y)$, is related simply to $\Delta\alpha_m$ and the previous reflection coefficient $\alpha_m^{[k-1]}(y)$:

$$\alpha_m^{[k]}(y) = \alpha_m^{[k-1]}(y)(1 + \Delta\alpha_m), \tag{2.15}$$

where the superscripts again represent nonlinear iteration index.

2.2 Particular Implementation of LSJIMP

In Section 2.1 I introduced the LSJIMP method in general. In the following section, I outline my particular implementation of the LSJIMP method. I start in Section 2.2.1 by extending the normal moveout (NMO) equation to image pegleg multiples in a prestack sense. In Sections 2.2.6-2.2.7 I introduce HEMNO (Heterogeneous Earth Multiple NMO Operator), a model-based multiple imaging operator which images peglegs in moderately heterogeneous geologic environments. In Sections 2.2.2-2.2.5 I present amplitude correction operators which model multiple events in the data from an image of the multiples. Finally, in Section 2.2.9, I outline how this particular imaging methodology for multiples fits into the LSJIMP methodology.

2.2.1 Kinematic imaging of pegleg multiples in a laterally-homogeneous earth

In a "1-D Earth" (horizontally-stratified, $v(z)$ medium), the normal-moveout (NMO) equation (Taner and Koehler, 1969) describes the prestack traveltime curve of a primary reflection at relatively short source-receiver offset:

$$t = \sqrt{\tau + \frac{x^2}{V_{\text{rms}}^2(\tau)}}. \tag{2.16}$$

Applied as an offset-dependent vertical time shift to a CMP gather, the NMO equation flattens an arbitrary primary to its zero-offset traveltime τ, where (half) offset is denoted x and the root-mean-square (RMS) velocity, $V_{\text{rms}}(\tau)$, is defined in a laterally-homogeneous earth as:

$$V_{\text{rms}}^2 = \frac{1}{\tau} \sum_{i=1}^{n_\tau} v_i^2 \Delta\tau \tag{2.17}$$

The earth is parameterized by n_τ layers of time thickness $\Delta\tau$, with constant interval velocity v_i in each layer.

Analogously, a modified NMO equation can image pegleg multiples in a 1-D Earth, as motivated graphically by Figure 2.3. From the figure, we see that kinematically, a first-order pegleg can be conceptualized as a "pseudo-primary" with the same offset, but with an additional two-way zero-offset traveltime to the multiple generator, τ^*. In equation form, let us extend this intuition to the general case of a j^{th}-order pegleg to write an NMO equation for peglegs:

$$t = \sqrt{(\tau + j\tau^*)^2 + \frac{x^2}{V_{\text{eff}}^2}}. \tag{2.18}$$

V_{eff} is the effective RMS velocity of the pseudo-primary shown in Figure 2.3. To derive an expression for V_{eff}, we modify the definition of RMS velocity, equation (2.17), to reflect a

j^{th}-order pegleg multiple's additional travel between the surface and multiple generator:

$$V_{\text{eff}}^2 = \frac{1}{\tau + j\tau^*}\left(j\sum_{i=1}^{n_{\tau^*}} v_i^2 \Delta\tau + \sum_{i=1}^{n_\tau} v_i^2 \Delta\tau\right). \tag{2.19}$$

Analogously, n_{τ^*} is the number of assumed layers between the earth's surface and the multiple generator. Notice that the two terms inside the parentheses of equation (2.19) are simply the definition of RMS velocity at τ^* and τ, respectively. We can substitute equation (2.19) accordingly to derive the final expression for $V_{eff}(\tau)$:

$$V_{\text{eff}}^2 = \frac{\left(j\tau^* V_{\text{rms}}^2(\tau^*) + \tau V_{\text{rms}}^2(\tau)\right)}{\tau + j\tau^*}. \tag{2.20}$$

Wang (2003) derives a similar series of expressions.

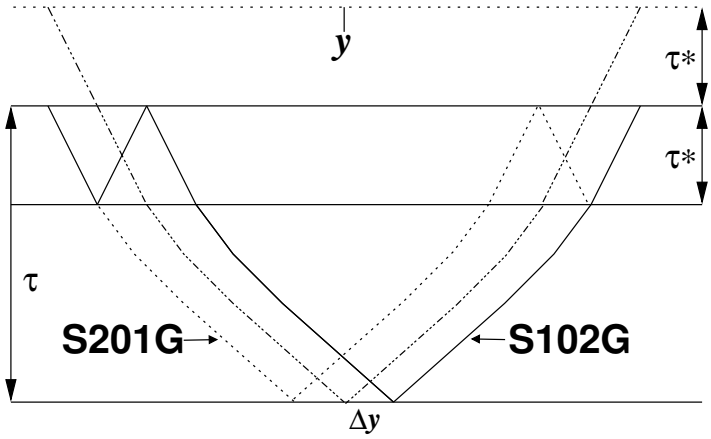

Figure 2.3: Pegleg multiples "S201G" and "S102G" have the same traveltimes as "pseudo-primary" with the same offset and an extra zero-offset traveltime τ^*. theory2d-schem [NR]

2.2.2 Amplitude corrections for pegleg multiples

It is tempting, but false, to believe that after scaling a pegleg by the reflection coefficient of the multiple generator, the event is directly comparable to a primary reflection. Primaries and their respective multiples traverse different raypaths between source and receiver, and thus exhibit different amplitude-versus-offset (AVO) behavior and suffer different anelastic attenuation and geometric spreading losses. In section 2.2.3 I derive the time- and offset-dependent

"Snell Resampling" operator to normalize peglegs to their primary with respect to AVO and attenuation. In section 2.2.4 I present a differential geometric spreading correction for peglegs, and finally, in section 2.2.5 I present an algorithm to estimate and apply the multiple generator's spatially-variant reflection coeffiecient.

2.2.3 Snell Resampling Normalizes AVO/Attenuation

Figure 2.4 illustrates the fact that in a $v(z)$ medium, there exists a single offset x_p such that a pegleg with offset x and primary with offset x_p are physically invariant with respect to AVO behavior and, assuming perfect elasticity in the top layer (often water), to anelastic attenuation. Since the pegleg multiple and primary in Figure 2.4 have the same emergence angle, θ, the time dip, or "stepout" of the two events is the same at x and x_p. In Appendix B, I derive the following expression for x_p, where V_{rms}, τ^*, and V_{eff} were defined in Section 2.2.1:

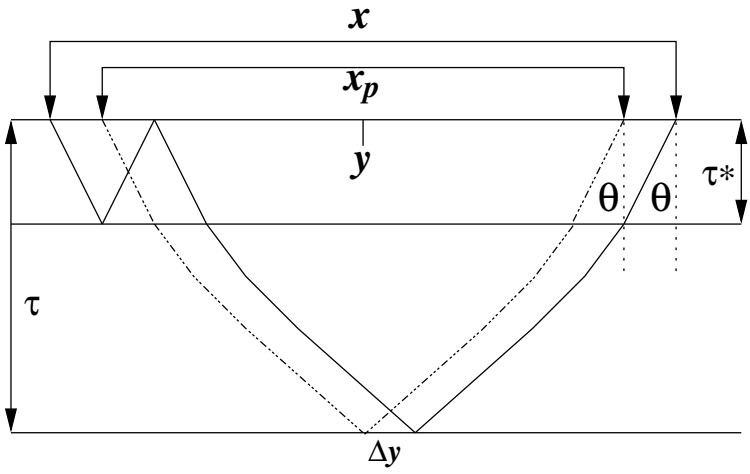

Figure 2.4: A primary and pegleg multiple with the same emergence angle (θ) and midpoint (y). Note different offsets (x and x_p) and a shift (Δy) in reflection point. theory2d-schem-snell [NR]

$$x_p = \frac{x\tau V_{\text{rms}}^2}{\sqrt{(\tau + j\tau^*)^2\ V_{\text{eff}}^4\ +\ x^2(V_{\text{eff}}^2 - V_{\text{rms}}^2)}}. \tag{2.21}$$

Equation (2.21) defines, for a j^{th}-order pegleg, a time-variable compression of the offset axis, which I denote "Snell Resampling". The name is derived from Ottolini's (1982) "Snell Traces" – a resampling of multi-offset reflection data along curves of constant stepout. Note that in

a constant velocity medium, $V_{\text{eff}} = V_{\text{rms}} = V$, and equation (2.21) reduces to the radial trace resampling used by Taner (1980) for the long-period deconvolution of peglegs.

Figure 2.5 illustrates application of Snell Resampling to a synthetic CMP gather. From the Figure, we see that Snell Resampling is an important vehicle for the exploitation of the additional information contained in the multiples. Notice how energy from the multiples is spread into the coverage gaps at near offsets and at 1.0 km offset. Snell Resampling moves energy from the multiples to the offset corresponding to its reflection angle at the target.

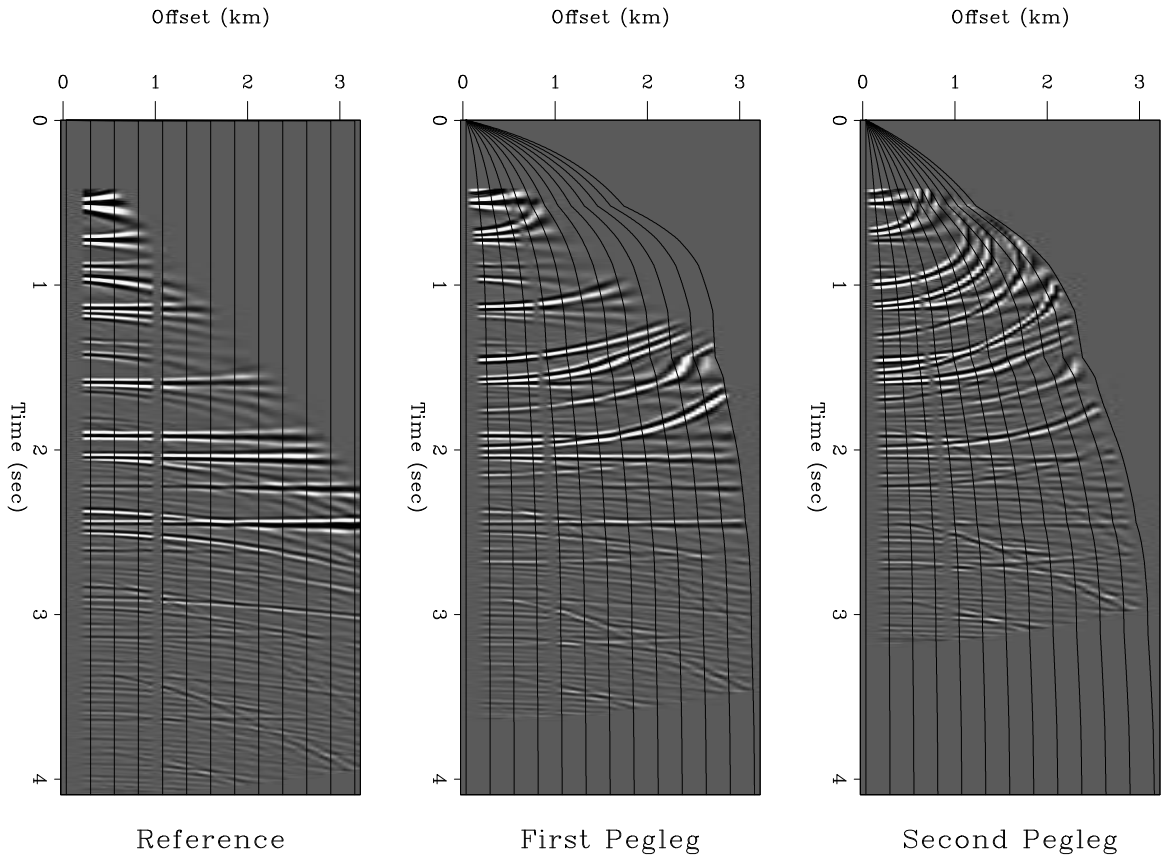

Figure 2.5: Snell Resampling demonstration. Left to right: a synthetic CMP gather after NMO for primaries and for first- and second-order peglegs, respectively. Snell Resampling (plus normalization to account for offset axis compression) was applied to the right two panels. The black lines illustrate the transformation's horizontal compression. The raw data has five unrecorded near offset traces and two dead traces at medium offsets. theory2d-snell.hask [CR,M]

Graphically (Figure 2.4), we may infer that the shift in midpoint, Δy, of the reflection points of the primary and first-order pegleg is:

$$\Delta y = \left(x - x_p\right)/2. \tag{2.22}$$

As a function of time, Δy decreases asymptotically to zero at infinite depth from a maximum of $x/4$ at the seabed. The deeper the reflector, the smaller Δy becomes. Similar expressions may be easily derived for multiples of other types and orders.

For peglegs arising from sub-seabed reflectors, the assumption of perfect elasticity for the multiple bounce breaks down. To some extent, however, the additional attenuation suffered by the multiple can, to first order, be treated as a decrease in reflection coefficient.

2.2.4 Differential Geometric Spreading

To correct peglegs for the effects of greater geometric spreading losses, I follow previous authors (Ursin, 1990; Lu et al., 1999) and write offset-dependent geometric spreading corrections for a primary (g_{prim}) and its pegleg multiples (g_{mult}) in the following notation:

$$g_{\text{prim}} = v^* t_{\text{prim}}(x) = \sqrt{(\tau v^*)^2 + \left(\frac{x v^*}{V}\right)^2} \tag{2.23}$$

$$g_{\text{mult}} = v^* t_{\text{mult}}(x) = \sqrt{[(\tau + j\tau^*)v^*]^2 + \left(\frac{x v^*}{V_{\text{eff}}}\right)^2}. \tag{2.24}$$

v^* is the velocity at the surface. After scaling by $g_{\text{mult}}/g_{\text{prim}}$ and Snell resampling, the amplitudes of an imaged pegleg multiple and its associated primary are consistent, to within a reflection coefficient.

2.2.5 Estimation/Application of Seabed Reflection Coefficient

After a pegleg multiple has been imaged, and undergone Snell Resampling and the differential geometric spreading correction, it is consistent with its primary to within the reflection coefficient of the multiple generator. In practice, the reflection coefficient always varies with space and reflection angle, though in many geologic environments these variations are both spatially smooth and small in magnitude.

In this thesis, I assume that the reflection coefficient varies in space, but does not vary with reflection angle. Assume that $\mathbf{p}(t,x,y)$ and $\mathbf{m}(t,x,y)$ are, respectively, small windows in time, offset, and midpoint of dimension $nt \times nx \times ny$, around a primary reflection and its first pure multiple after normalized Snell Resampling and differential geometric spreading correction. The reflection coefficients, $\mathbf{r}(y)$, are chosen to minimize the following quadratic functional:

$$\min_{\mathbf{r}(y)} \sum_{k=1}^{ny} \sum_{j=1}^{nx} \sum_{i=1}^{nt} \mathbf{w}(k)^2 \left[\mathbf{r}(k)\, \mathbf{p}(i,j,k) - \mathbf{m}(i,j,k)\right]^2 + \epsilon^2 \sum_{k=2}^{ny} [\mathbf{r}(k) - \mathbf{r}(k-1)]^2 . \quad (2.25)$$

The second term, a finite-difference first derivative applied to the unknown $\mathbf{r}(y)$, enforces a degree of smoothness across midpoint. The scalar term ϵ balances data fitting with model smoothness. The vector of residual weights, $\mathbf{w}(y)$, reflect the "quality" of the data at y.

Recall from Figure 2.4 that for a multiple and primary recorded at the same midpoint, there exists a shift in the target reflection point, Δy, described by equation (2.22) for a first-order pegleg. In my LSJIMP implementation, variations in reflection strength of the target reflector are ignored, but not those in the multiple generator. A first justification of this assumption is convenience: the strength of the target reflection is, after all, unknown. Secondly, since the target reflection points of all legs of a pegleg are symmetric about the midpoint, the average of the reflection stregths is the same as the primary's if the true reflection strength is locally linear with midpoint. Δy decreases with target depth, so for deep targets the local linearity assumption is likely to hold to first-order accuracy. Thirdly, ignoring target reflector variation implies that the model space of the LSJIMP inversion consists of one midpoint location only, which reduces memory usage and permits coarse-grained computer parallelization over midpoints. Therefore, when applying the reflection coefficient, we apply the coefficient at the assumed

reflection point for the particular multiple being imaged. Second order multiples would be scaled by reflection coefficients from two locations, and so on.

2.2.6 HEMNO: Imaging of pegleg multiples in a heterogeneous earth

In Sections 2.2.1-2.2.5 I developed a methodology, valid in a laterally-homogenous earth, to image pegleg multiples and make their amplitudes comparable to their primary. From Figure 2.3, recall that a first-order pegleg consists of two unique arrivals: the event with a multiple bounce over the source ("source-side" pegleg), and the event with a bounce over the receiver ("receiver-side" pegleg). When reflectors dip, the arrivals have different traveltimes on a CMP gather, and "split" into two separate events. Figure 2.6 illustrates the splitting phenomenon on the 2-D Gulf of Mexico dataset which will be used extensively in Chapter 3. The strong events in the "crosshairs" of the Figure are the first-order source-side and receiver-side seabed pegleg multiples from the top of salt reflection.

On CMP gathers, primary reflection hyperbolas generally have apexes at zero offset. Levin and Shah (1977) show that the apexes of split pegleg multiples shift away from zero offset, raising the apparent velocity of one leg (on one-sided marine data), which can hamper velocity analysis and Radon multiple suppression. Hargreaves et al. (2003) use an apex-shifted Radon transform for demultiple.

Even if reflectors dip only mildly, a prestack imaging method for peglegs must account for splitting. Mild variations in reflector depth over a cable length can introduce considerable destructive interference between the legs of a pegleg multiple at far offsets. This interference, is impossible to model with a 1-D theory, introduces false amplitude-versus-offset (AVO) behavior in the multiples, and certainly would hamper any attempts to use multiples as a constraint on the AVO signature of the primaries (Levin, 1996).

Levin and Shah (1977) deduced analytic kinematic moveout equations for split 2-D pegleg multiples, and Ross et al. (1999) extended the work to 3-D. Both approaches assume constant velocity and locally planar reflectors – depending on local geology, this may be unrealistic in practice. In this thesis, my particular implementation of LSJIMP relies on a simplified

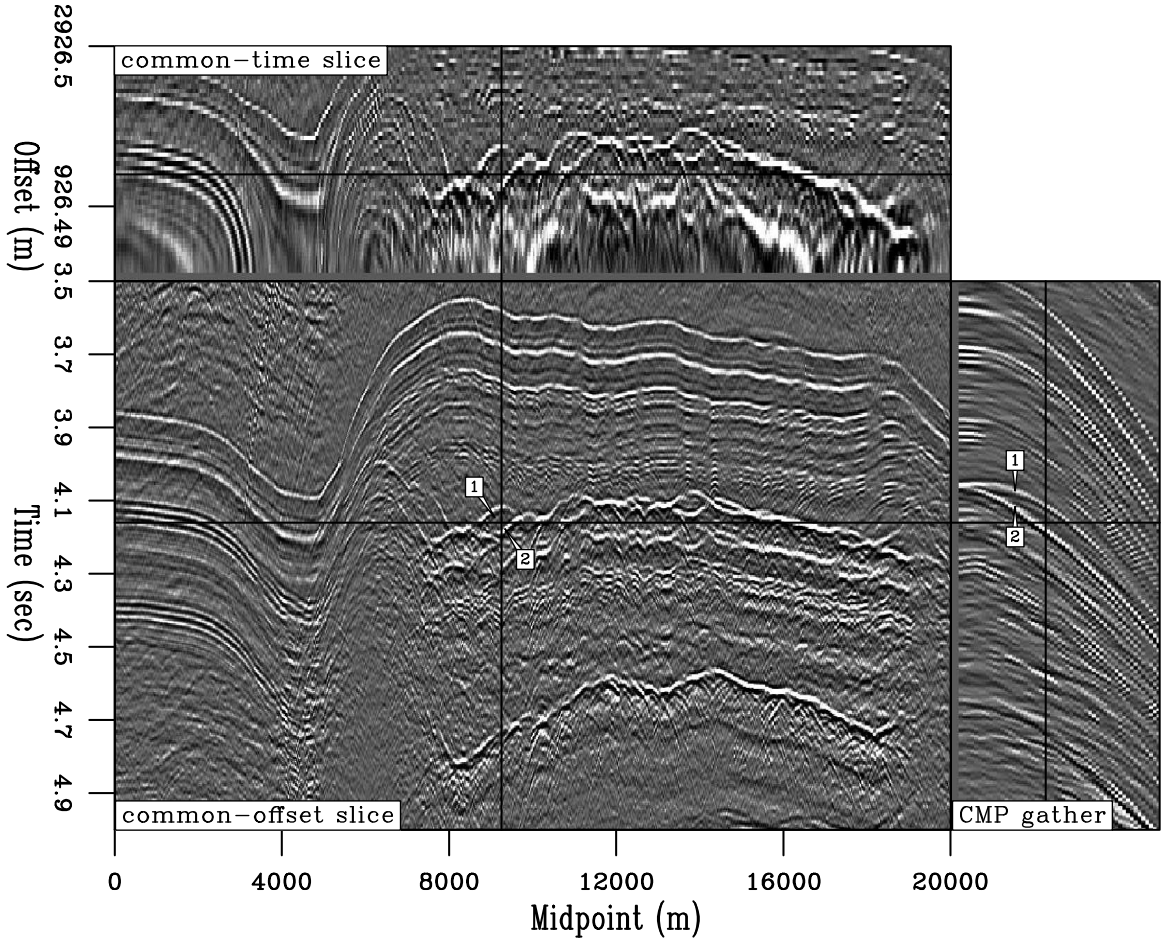

Figure 2.6: Splitting phenomenon observed on 2-D prestack field data from the Gulf of Mexico (used in Chapter 3). The seabed pegleg from the top of salt reflection splits noticeably into two distinct events (labels "1" and "2"). On the CMP gather the apexes of the two legs are shifted away from zero offset. theory2d-gulf.split [ER]

moveout equation based upon a more practically realizable conceptual model, which I call HEMNO (Heterogeneous Earth Multiple NMO Operator). In Appendix A I prove that for small reflector dips, the HEMNO traveltime equation reduces to Levin and Shah's moveout equations.

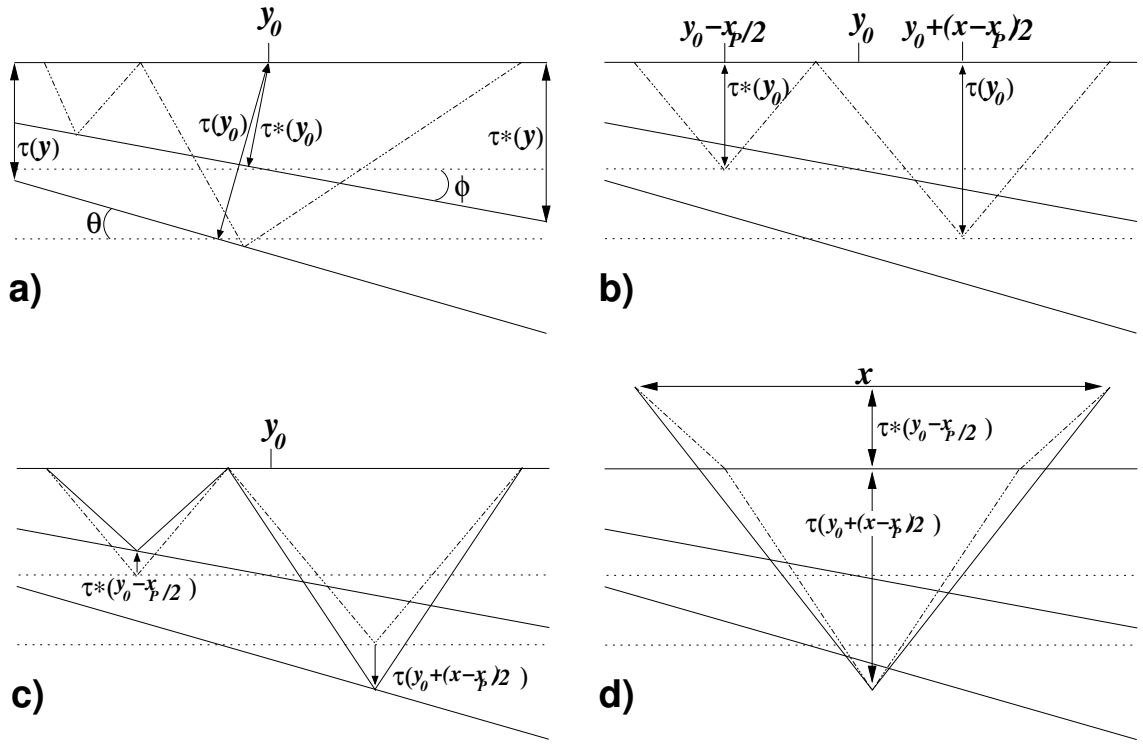

Figure 2.7: HEMNO operator schematic. (a) True raypath in constant-velocity earth. The zero-offset traveltimes to the seabed and subsea reflector are $\tau^*(y_0)$ and $\tau(y_0)$, respectively. (b) Assumed reflection points under flat-earth assumption. x_p is defined in equation (2.21). (c) Stretch legs of raypath vertically to match measured $\tau^*(y_0 - x_p/2)$ and $\tau(y_0 + (x - x_p)/2)$. Panel (d) Connect legs of raypath. The solid line that connects the reassembled raypath is the final result. theory2d-schem-pegleg-dip2 [NR]

Figure 2.7 graphically illustrates the HEMNO derivation in a constant-velocity earth. Panel a) illustrates the raypath of the "S102G" pegleg where the multiple generator and target reflector dip. Panel b) illustrates the raypath implied by the 1-D multiple imaging theory derived in Section 2.2.1: the primary leg of the multiple has offset x_p [equation (2.21)] and the zero-offset traveltime to both reflectors is spatially invariant. Panel c) illustrates the HEMNO strategy: we account for spatially-variant reflector geometry by vertically stretching the 1-D

raypath to match the zero-offset traveltime at the reflection points. However, the solid raypath in panel c) disobeys Snell's Law, so to obtain the final result in panel d), the tails of the legs of the ray are simply connected to produce a valid raypath, which has the equation of a hyperbola with offset x and zero-offset traveltime $\tau^*(y_0 - x_p/2) + \tau(y_0 + (x - x_p)/2)$. We first define for simplicity

$$\tau_m = \tau^*(y_0 - x_p/2) \quad \text{and} \quad \tau_p = \tau(y_0 + (x - x_p)/2), \tag{2.26}$$

and then write the HEMNO equation:

$$t^2 = \left(\tau_m + \tau_p\right)^2 + \frac{x^2}{V_{\text{eff}}^2}. \tag{2.27}$$

Equation (2.27) flattens one leg of a first-order pegleg in offset and shifts the event to the zero-offset traveltime of the primary. By using V_{eff}, we ignore lateral velocity variations, which is consistent with the assumption of small dips. Similar expressions may be derived for other multiple events, but I omit the derivations for brevity. Figure 2.8 illustrates application of the HEMNO equation to the split top of salt pegleg shown in Figure 2.6.

2.2.7 HEMNO Implementation Issues

To implement equation (2.27) on a computer, we must obtain two quantities. The first, the zero-offset traveltime of the multiple generator, τ_m, may be obtained by hand- or auto-picking, and optionally refined by cross-correlation. However, the second quantity, the zero-offset traveltime to an arbitrary target reflector, τ_p , cannot realistically be picked. I obtain τ_p automatically by event tracking, using a smooth estimate of reflector dip obtained from a zero-offset section, in a fashion similar to Lomask's (2003) data flattening method.

How to best obtain this dip estimate is a question still open to debate. Automatic dip estimation techniques like Fomel's (2002) yield good results in regions where reflectors are densely packed, coherent, and do not cross. Unfortunately, below the onset of the first seabed

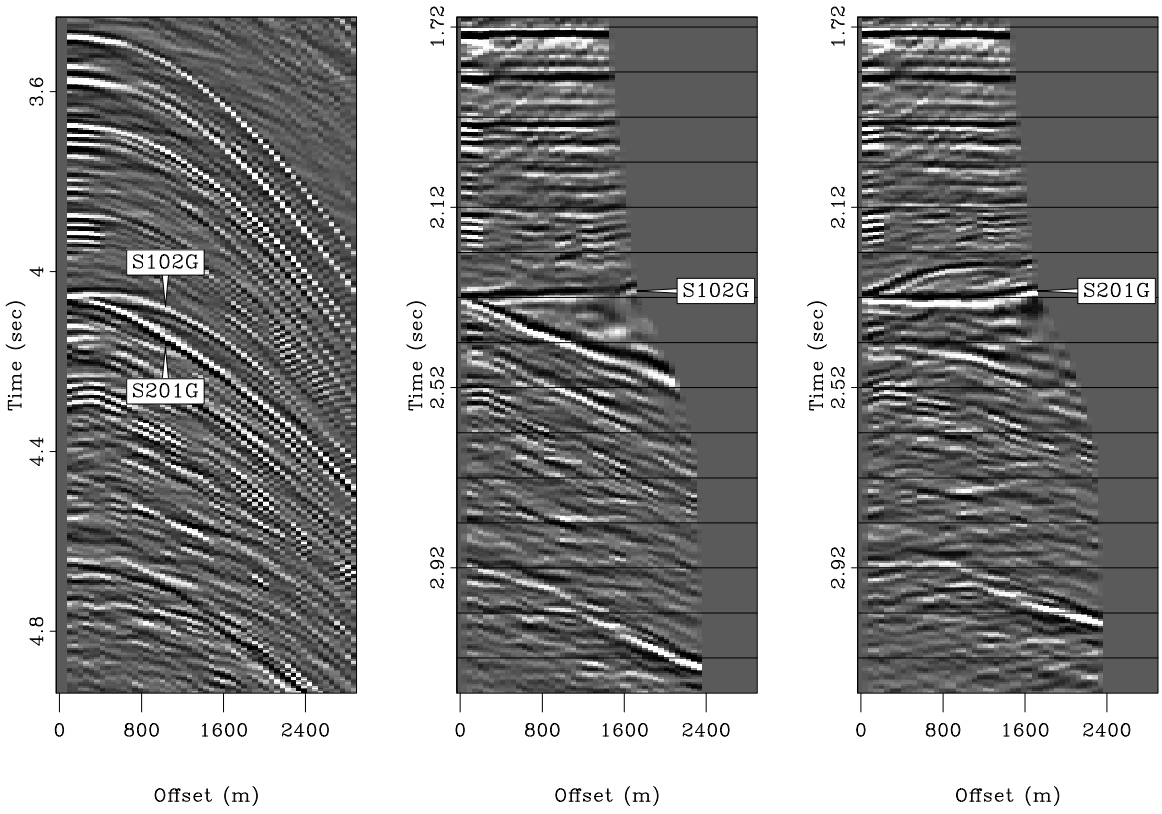

Figure 2.8: Left: CMP gather extracted from midpoint 9200 m of the Mississippi Canyon data cube shown in Figure 2.6. Notice the split top of salt pegleg at $\tau = 4.05s$. Center and Right: HEMNO equation applied to two splits. Notice how the events are independently focused in time and offset. The images panels have also undergone normalized Snell Resampling, differential geometric spreading correction, and application of the seabed reflection coefficient. theory2d-gulf.hemno.split [CR]

multiple, a zero-offset section will contain crossing events. While previous authors have developed methods to simultaneously estimate two crossing dips (Fomel, 2001; Brown, 2002), the problem is highly nonlinear, and it is difficult to unambiguously associate one dip with the primaries, and the other with multiples.

I have had greater success with a different technique which exploits cubic smoothing splines (Hutchinson and De Hoog, 1985). On 2-D data, it is easy to pick important reflectors on a zero-offset section, even weak events buried under the multiples. The reflectors are first fit with a cubic smoothing spline, from which the dip, simply the first derivative, can be computed analytically. These computed dips are finally interpolated in time, again using a cubic smoothing spline. This method is somewhat manually intensive, but gives reliable results. In 3-D, the spline technique may have value when crossline aliasing renders automatic dip estimation schemes ineffective. If the data contain many important reflectors, though, the picking may entail considerable manual labor.

2.2.8 Velocity-Depth Ambiguity in the Imaging of Multiples

As shown in Figure 2.7, the HEMNO approach for imaging pegleg multiples that I introduced in section 2.2.6 assumes that the reflection points of multiples do not move in midpoint from their "1-D Earth" position. This assumption is violated in the presence of nonzero reflector dip or lateral velocity variation. Reflector dip affects the kinematic properties of multiples in two ways, which were quantified by Levin (1971) in a seminal paper. First, dip always leads to a negative shift in the zero-offset traveltime of multiples relative to the 1-D case. Second, multiples from dipping reflectors always have a higher apparent velocity than those from flat reflectors.

Prestack migration methods naturally and automatically unravel the mystery of dip to correct seismic data for the effects of nonzero offset. However, HEMNO is a more mechanical operation. To image a multiple, it requires an estimate of zero-offset traveltime and the multiple's stacking velocity. Unfortunately, these quantities are inherently coupled. The goal of HEMNO is to "best" align a multiple and its primary as a function of offset. A small perturbation in τ^* may better align the multiple and primary at zero offset, but will change the

multiple's apparent velocity and possibly worsen alignment at far offsets. Conversely, if a multiple is nonflat after imaging, a small velocity perturbation may improve far-offset alignment but will not change near-offset alignment.

In this thesis I take a pragmatic view of the velocity-depth ambiguity problem. Pure multiples do not split. If a primary is flat after imaging, but its pure multiple is not, then any residual moveout in the multiple is due to dip and/or lateral velocity variation. I use a two-step process to handle the nonlinear coupling of velocity and reflector position:

1. Compute perturbation in τ^* by aligning near-offset stacks of primary and its pure multiple with a cross-correlation approach (Rickett and Lumley, 2001).

2. Compute perturbation in multiple velocity by performing residual stacking velocity analysis for the (pure) multiple event of interest. The velocity perturbation is applied for all τ in V_{eff} [equation (2.20)].

2.2.9 Solving the particular LSJIMP problem

Now that we have derived appropriate imaging and amplitude correction operators, we are ready to translate the general LSJIMP modeling equation (2.2) to my particular implementation. The primary image, $\mathbf{m}_0$, is mapped into data space primary events by NMO, $\mathbf{N}_0$. Similarly, a given pegleg image, $\mathbf{m}_{i,k,m}$, is mapped into data space by sequentially applying the differential geometric spreading correction ($\mathbf{G}_{i,m}$), Snell resampling ($\mathbf{S}_{i,m}$), HEMNO ($\mathbf{N}_{i,k,m}$), and finally, a reflection coefficient ($\mathbf{R}_{i,k,m}$). Let us rewrite equation (2.2) accordingly:

$$\mathbf{d}_{\text{mod}} = \mathbf{N}_0\mathbf{m}_0 + \sum_{i=1}^{p}\sum_{k=0}^{i}\sum_{m=1}^{n_{\text{surf}}} \mathbf{R}_{i,k,m}\mathbf{N}_{i,k,m}\mathbf{S}_{i,m}\mathbf{G}_{i,m}\mathbf{m}_{i,k,m}\,. \tag{2.28}$$

We see that in equation (2.28), the analog to $\mathbf{L}_{i,k,m}$ in equation (2.2) is $\mathbf{R}_{i,k,m}\mathbf{N}_{i,k,m}\mathbf{S}_{i,m}\mathbf{G}_{i,m}$.

The data residual weight in equation (2.5), $\mathbf{W_d}$, can often strongly influence the success of the inversion. Technically, $\mathbf{W_d}$ carries a heavy burden: it must decorrelate and balance the residual. However, I have found that a simpler form for $\mathbf{W_d}$ nontheless pays dividends. I set

$\mathbf{W_d}$, which has the same dimension as a CMP gather, to zero where the data, $\mathbf{d}$, has an empty trace, and also above the onset of the seabed reflection.

Bibliography

AAPG, 1998, Gulf of mexico petroleum systems: AAPG Bulletin, **82**, no. 5.

Berkhout, A. J., and Verschuur, D. J., 1994, Multiple technology: Part 2, migration of multiple reflections: Soc. of Expl. Geophys., 64th Ann. Internat. Mtg, 1497–1500.

Berkhout, A. J., and Verschuur, D. J., 2003, Transformation of multiples into primary reflections:, *in* 73rd Ann. Internat. Mtg Soc. of Expl. Geophys.

Berryhill, J. R., and Kim, Y. C., 1986, Deep-water peglegs and multiples - Emulation and suppression: Geophysics, **51**, no. 12, 2177–2184.

Biondi, B., and Palacharla, G., 1996, 3-D prestack migration of common-azimuth data: Geophysics, **61**, no. 06, 1822–1832.

Biondi, B., Fomel, S., and Chemingui, N., 1998, Azimuth moveout for 3-D prestack imaging: Geophysics, **63**, no. 02, 574–588.

Biondi, B., 1997, Azimuth moveout + common-azimuth migration: Cost-effective prestack depth imaging of marine data: Soc. of Expl. Geophys., 67th Ann. Internat. Mtg, 1375–1378.

Brown, M., 2002, Simultaneous estimation of two slopes from seismic data, applied to signal/noise separation: SEP–**112**, 181–194.

Claerbout, J. F., 1992, Earth Soundings Analysis: Processing Versus Inversion: Blackwell Scientific Publications.

Claerbout, J. F., 1995, Basic Earth Imaging: Stanford Exploration Project.

Fomel, S., 2001, Three-dimensional seismic data regularization: Ph.D. thesis, Stanford University.

Fomel, S., 2002, Applications of plane-wave destruction filters: Geophysics, **67**, no. 06, 1946–1960.

Foster, D. J., and Mosher, C. C., 1992, Suppression of multiple reflections using the Radon transform: Geophysics, **57**, no. 03, 386–395.

Guitton, A., Brown, M., Rickett, J., and Clapp, R., 2001, Multiple attenuation using a t-x pattern-based subtraction method: Soc. of Expl. Geophys., 71st Ann. Internat. Mtg, 1305–1308.

Guitton, A., 2002, Shot-profile migration of multiple reflections: 72nd Ann. Internat. Mtg., Soc. of Expl. Geophys., Expanded Abstracts, 1296–1299.

Hampson, D., 1986, Inverse velocity stacking for multiple elimination: J. Can. Soc. Expl. Geophys., **22**, no. 01, 44–55.

Hargreaves, N., Wombell, R., and VerWest, B., 2003, Multiple attenuation using an apex-shifted radon transform: 65th Mtg., Eur. Assoc. Geosc. Eng., Workshop: Strategies Towards Multi-Dimensional Multiple Attenuation.

He, R., and Schuster, G., 2003, Least-squares migration of both primaries and multiples:, *in* 73rd Ann. Internat. Mtg Soc. of Expl. Geophys.

Hokstad, K., and Sollie, R., 2003, 3-D surface-related multiple elimination using parabolic sparse inversion:, *in* 73rd Ann. Internat. Mtg Soc. of Expl. Geophys., 1961–1964.

Hutchinson, M., and De Hoog, F., 1985, Smoothing noisy data with spline functions: Smoothing noisy data with spline functions:, Numer. Math., 99–106.

Kabir, M. M. N., and Marfurt, K. J., 1999, Toward true amplitude multiple removal: The Leading Edge, **18**, no. 1, 66–73.

Kleemeyer, G., Pettersson, S., Eppenga, R., Haneveld, C., Biersteker, J., and Den Ouden, R., 2003, It's magic – industry first 3D surface multiple elimination and pre-stack depth migration on Ormen Lange:, *in* 65th Mtg. Eur. Assn. Geosci. Eng., Session:B–43.

Kuehl, H., and Sacchi, M., 2001, Generalized least-squares DSR migration using a common angle imaging condtion: Soc. of Expl. Geophys., 71st Ann. Internat. Mtg, 1025–1028.

Levin, F. K., and Shah, P. M., 1977, Peg-leg multiples and dipping reflectors: Geophysics, **42**, no. 05, 957–981.

Levin, F. K., 1971, Apparent velocity from dipping interface reflections: Geophysics, **36**, no. 03, 510–516.

Levin, S. A., 1996, AVO estimation using surface-related multiple prediction: Soc. of Expl. Geophys., 66th Ann. Internat. Mtg, 1366–1369.

Lomask, J., 2003, Flattening 3D seismic cubes without picking: Soc. of Expl. Geophys., 73rd Ann. Internat. Mtg., 1402–1405.

Lu, G., Ursin, B., and Lutro, J., 1999, Model-based removal of water-layer multiple reflections: Geophysics, **64**, no. 6, 1816–1827.

Morley, L., 1982, Predictive multiple suppression: Ph.D. thesis, Stanford University.

Nemeth, T., Wu, C., and Schuster, G. T., 1999, Least-squares migration of incomplete reflection data: Geophysics, **64**, no. 1, 208–221.

Ottolini, R., 1982, Migration of reflection seismic data in angle-midpoint coordinates: Ph.D. thesis, Stanford University.

Paffenholz, J., 2003, All-azimuth streamer acquisition: the impact on 3D multiple attenuation: 65th Mtg., Eur. Assoc. Geosc. Eng., Workshop: Strategies Towards Multi-Dimensional Multiple Attenuation.

Prucha, M. L., and Biondi, B. L., 2002, Subsalt event regularization with steering filters: 72nd Ann. Internat. Mtg., Soc. of Expl. Geophys., Expanded Abstracts, 1176–1179.

Prucha-Clapp, M., and Biondi, B., 2002, Subsalt event regularization with steering filters: Soc. of Expl. Geophys., 72nd Ann. Internat. Mtg, 1176–1179.

Reiter, E. C., Toksoz, M. N., Keho, T. H., and Purdy, G. M., 1991, Imaging with deep-water multiples: Geophysics, **56**, no. 07, 1081–1086.

Rickett, J., and Lumley, D. E., 2001, Cross-equalization data processing for time-lapse seismic reservoir monitoring: A case study from the Gulf of Mexico: Geophysics, **66**, no. 4, 1015–1025.

Riley, D. C., and Claerbout, J. F., 1976, 2-D multiple reflections: Geophysics, **41**, no. 04, 592–620.

Ross, W. S., Yu, Y., and Gasparotto, F. A., 1999, Traveltime prediction and suppression of 3-D multiples: Geophysics, **64**, no. 1, 261–277.

Sacchi, M. D., and Ulrych, T. J., 1995, High-resolution velocity gathers and offset space reconstruction: Geophysics, **60**, no. 04, 1169–1177.

Sava, P., and Fomel, S., 2000, Angle-gathers by Fourier Transform: SEP–**103**, 119–130.

Sava, P., and Fomel, S., 2003, Angle-domain common-image gathers by wavefield continuation methods: Geophysics, **68**, no. 3, 1065–1074.

Shan, G., 2003, Source-receiver migration of multiple reflections:, *in* 73rd Ann. Internat. Mtg Soc. of Expl. Geophys.

Shuey, R. T., 1985, A simplification of the Zoeppritz-equations: Geophysics, **50**, no. 04, 609–614.

Stoffa, P. L., Fokkema, J. T., de Luna Freire, R. M., and Kessinger, W. P., 1990, Split-step Fourier migration: Geophysics, **55**, no. 4, 410–421.

Taner, M. T., and Koehler, F., 1969, Velocity spectra - Digital computer derivation and applications of velocity functions: Geophysics, **34**, no. 06, 859–881.

Taner, M. T., 1980, Long-period sea-floor multiples and their suppression: Geophys. Prosp., **28**, no. 01, 30–48.

Tarantola, A., 1984, Inversion of seismic reflection data in the acoustic approximation: Geophysics, **49**, no. 08, 1259–1266.

Thorson, J. R., and Claerbout, J. F., 1985, Velocity stack and slant stochastic inversion: Geophysics, **50**, no. 12, 2727–2741.

Tsai, C. J., 1985, Use of autoconvolution to supress first-order long-period multiples: Use of autoconvolution to supress first-order long-period multiples:, Soc. of Expl. Geophys., Geophysics, 1410–1425.

Ursin, B., 1990, Offset-dependent geometrical spreading in a layered medium (short note): Geophysics, **55**, no. 04, 492–496.

van Borstelen, R., 2003, Optimization of marine data acquisition for the application of 3D SRME:, *in* 73rd Ann. Internat. Mtg Soc. of Expl. Geophys., 1965–1968.

van Dedem, E., and Verschuur, D., 2002, 3D surface-related multiple prediction using sparse inversion: experience with field data: Soc. of Expl. Geophys., 72nd Ann. Internat. Mtg, 2094–2097.

Verschuur, D. J., Berkhout, A. J., and Wapenaar, C. P. A., 1992, Adaptive surface-related multiple elimination: Geophysics, **57**, no. 09, 1166–1177.

Wang, J., Kuehl, H., and Sacchi, M. D., 2003, Least-squares wave-equation avp imaging of 3D common azimuth data:, *in* 73rd Ann. Internat. Mtg Soc. of Expl. Geophys.

Wang, Y., 2003, Multiple subtraction using an expanded multichannel matching filter: Geophysics, **68**, no. 1, 346–354.

Wiggins, J. W., 1988, Attenuation of complex water-bottom multiples by wave equation-based prediction and subtraction: Geophysics, **53**, no. 12, 1527–1539.

Yu, J., and Schuster, G., 2001, Crosscorrelogram migration of IVSPWD data: Soc. of Expl. Geophys., 71st Ann. Internat. Mtg, 456–459.